Detection of Porphyry Intrusions Using Analytic Signal (AS), Euler Deconvolution, and Center for Exploration Targeting (CET) Technique at Wadi Allaqi Area, South Eastern Desert, Egypt

Sayed O. Elkhateeb[b*1], Ahmed M. Eldosouky[a*2].

Abstract-- The present study is based on the enhancement of the Reduced to the pole Total magnetic intensity map of Wadi Allaqi area, South Eastern Desert, Egypt to delineate porphyry intrusions. Hydrothermal alteration associated with dyke-like structure comprises concentric near-circular alteration zones surrounding a roughly circular central intrusion. Aeromagnetic data of Wadi Allaqi area were processed using Analytic Signal (AS), Euler Deconvolution, and Center for Exploration Targeting (CET) Plug-In Porphyry Analysis. From the AS and Euler Deconvolution maps it can clearly notice that the major contact trends are WNW-ESE, NW-SE, and NE-SW directions with minor traces of N-S trend direction. It deserves mention to note that many of the causative sources in the study area appear as circular bodies. Also, they generally assume definite trends which means that they are structurally controlled. CET porphyry analysis map highlights the regions that can contain numerous occurrences of porphyry-style mineralization in Wadi Allaqi area. The predicated locations of CET porphyry intrusion closely match the locations of the known deposits in the area.

Keywords-- Reduced To The Pole Total Magnetic Intensity, Analytic Signal (AS), Euler Deconvolution, and Center for Exploration Targeting (CET).

IJSER

1 INTRODUCTION

Airborne geophysical surveying is the process of measuring the variation of different physical or geochemical parameter of the earth such as distribution of magnetic minerals, density, electrical conductivity and radioactive element concentration. The capability of modern airborne magnetic anomaly mapping, as one of several geophysical tools available to assist the geological mapping of largely concealed terrains underlining the high degree of sophistication achieved by technology in recent years (Reeves et al., 1997; Gunn, 1997; Reeves, 1998).

Maps of spatial variations in TMI, and products derived from transformations of this primary data type, are typically presented in raster form, i.e. as a grid of values, and are displayed as coloured images. The manual interpretation of magnetic images involves the correlation of observed features and patterns with those expected from the geological environment that comprises the survey area. That is, geoscientific knowledge is used to fit 'templates' to the observed responses in what is a subjective interpretational process. The magnetic data may be used to create a pseudo-geological map from which possible sites of mineralization may be inferred based on knowledge and opinion as to what are key controls on deposit formation. This process often requires detection of responses from edges or discontinuities that are associated with structures such as faults, dykes or lithological boundaries (Blakely and Simpson, 1986; Cella et al., 2009; Fedi, 2002).

Alternatively, and of most relevance here, the interpreter may seek magnetic responses from mineralization itself, alteration associated with the mineralized environment and/or some specific geological environment in which mineralization occurs. Massive nickel sulphide mineralization is an example of a deposit type where responses from the mineralization itself may be detected (Gunn and Dentith, 1997 and references therein). A good example of responses from a specific geological setting is the magnetic response from potentially diamondiferous kimberlites, e.g. Macnae (1995). Excellent examples of magnetic responses associated with alteration are those from porphyry-style mineralization where extensive areas of hydrothermal alteration often have different magnetism to the areas of unaltered geology. In this paper we apply an image analysis method for rapidly locating magnetic signatures typical of porphyry hydrothermal systems. The method generates indicative shapes of the detected porphyry systems by tracing feature boundaries at Wadi Allaqi area.

- Department of Geology, Faculty of Science, South Valley University, Egypt.[1]
- Egyptian Environmental Affairs Agency(E.E.A.A),Egypt.[2]

2 STUDY AREA

2.1. Location and Extent of the Study Area

Wadi Allaqi area lies in the South Eastern Desert of Egypt and represents part of the Neoproterozoic Arabian-Nubian Shield (Fig. 1) covering an area about 7050km². The area extends from latitudes 22° 22′50" to 23° 00′00"N and longitudes 33° 15′ to 34° 15′ E. The region is dominated by the western extension of the Allaqi-Heiani-Gerf-Onib-Sol Hamid-Yanbu suture (Stern et al., 1989; Stern, 1994; Abdelsalam and Stern, 1996).

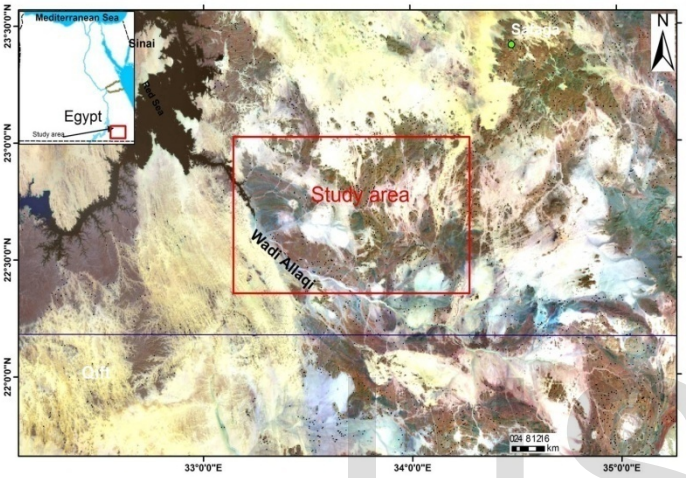

Fig. 1: Location map showing the study area.

2.2. Geology of Wadi Allaqi Area

The geological map of the study area (Fig. 2) shows that Wadi Allaqi area is underlain by Neoproterozoic crystalline rocks, Cretaceous sandstone, and Mesozoic and younger volcanic and sub-volcanic rocks. The Neoproterozoic rocks and associated hydrothermal deposits are the focus of this study. These rocks underlie most of the study area and consist of ophiolitic assemblage, island arc assemblage, and late- to post-tectonic granitic intrusions (Geologic map of Wadi Jabjabah Quadrangle, Egypt 1996).

South Western part of the study area is cover by Cretaceous Sandstone formations including Al Jilf formation, Abu Sumbul ormation, Al Burj formation, and Abu Ajjaj formation while Quaternary deposits fill Wadies of the area.

2.2.1. The Ophiolitic Assemblage

These rocks are scattered in the central part of the Wadi Allaqi area and are made up of imbricated thrust sheets and slices of serpentinites, talc carbonate schist, and metagabbros. These are thrust from north to south across the island-arc assemblage.

2.2.2. The Island-Arc Assemblage

This assemblage is represented by meta-sedimentary and metavolcanic layered units and intrusive gabbro to diorite plutons (Fig. 2). The geochemistry of some of these meta-volcanic rocks suggests transitional environment between continental arc and continental margin (El-Nisr, 1997). The gabbro-diorite intrusions of the island-arc assemblage are less abundant than the meta-sedimentary and metavolcanic units. These intrusions are heterogeneous in composition and include gabbro, diorite, quartz-diorite, and tonalite.

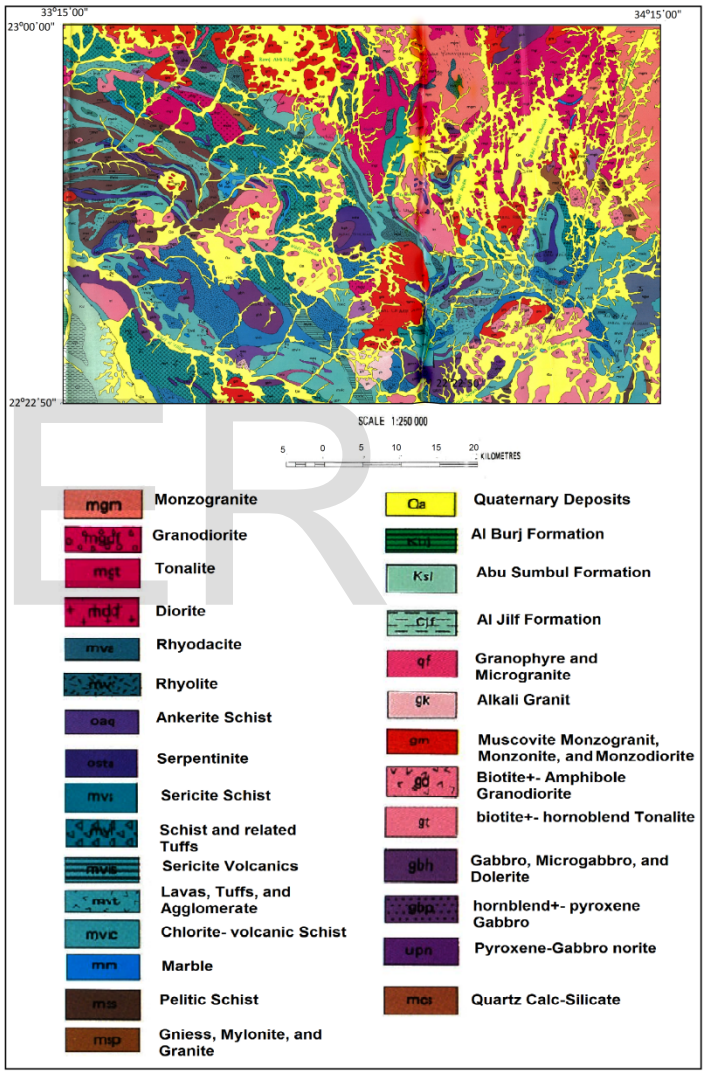

Fig. 2: Geologic map of the study area (by EGSMA., 1996).

2.2.3. The Late to Post-Tectonic Granitoids

Late- to post-tectonic granitic bodies are widespread in the central part of the study area, especially close to Wadi Umm Shelman (Fig. 2). They occur as deeply eroded, circular features with few isolated low-lying hills draped by Recent sand deposits. Post-tectonic granitic bodies are widely

distributed in the northern part of the study area . They are massive, medium in grain size, and red in color with high to medium relief. They intruded the above rock unites and are cut by felsic intrusions as well as felsic and mafic dikes.

2.3. Tectonic Setting

The Neoproterozoic basement rocks in northeastern Africa and eastern Arabia comprise the Arabian-Nubian Shield, which is made up of intra-oceanic island-arc and back-arcbasin complexes and micro-continents welded together along north- to east-trending sutures and disrupted by north- and northwestern-trending post-accretionary shear zones (Stern, 1994; Abdelsalam and Stern, 1996). One of these sutures is the east- to northeast-trending Allaqi-Heiani-Onib-Sol Hamed- Yanbu suture (Stern et al., 1990). The western part of this suture is exposed north of Wadi Allaqi and is the focus of this study. The suture in northeastern Sudan and southeastern Egypt separates the Southeastern Desert terrane in the north from the 830 to 720-Ma Hijaz-Gebeit-Gabgaba-Halfa terrane to the south.

3 MATERIALS AND METHODS

3.1. Aeromagnetic data

The magnetic data used in this study was obtained from the Egyptian Mineral Resources Authority collected by Aero Service Company (1983). Aeromagnetic surveys were flown with a flight height of 120 m and the average magnetic inclination was 32.8 N and declination was 1.9 E.

The reduced to pole total magnetic intensity (RTP-TMI) map (Fig. 5) was derived from total magnetic intensity map of the study area after subtracting the theoretical geomagnetic field or IGRF (International Geomagnetic Reference Field).

3.2. Methods

The procedures employed in this research include:

1. Production of Reduced To Pole Total Magnetic Intensity (RTP-TMI) map of the study area.
2. Computing of Analytic Signal of RTP_TMI.
3. Computing Euler Deconvolution of RTP-TMI.
4. Application of Center for Exploration Targeting (CET) Porphyry Analysis Plug-In for Structural Analysis.

3.3. Theory of Method

3.3.1. Analytic Signal (AS)

The analytic signal (Nabighian, 1972, 1984; Roest et al., 1992) is a function related to magnetic fields by the derivatives:

$$AS = \sqrt{\left(\frac{\partial A}{\partial X}\right)^2 + \left(\frac{\partial A}{\partial Y}\right)^2 + \left(\frac{\partial A}{\partial Z}\right)^2} \quad (1)$$

This function is extremely interesting in the context of interpretation, in that it is completely independent of the direction of the magnetization and the Earth's magnetic field. This means that all bodies with the same geometry have the same analytic signal. The analytical signal displays maxima over the source body edges even when the direction of the magnetization is not vertical. Furthermore as the peaks of analytic signal functions are symmetric and occur directly over the edges of wide bodies and directly over centers of narrow bodies, interpretation of analytic signal maps and images should, in principle, provide simple, easily understood indications of magnetic source geometry, the half widths of these peaks can be linearly related to depths, if the sources of the peaks are vertical magnetic contacts (Roest et al., 1992).

The analytic signal, although often more discontinuous than the simple horizontal gradient, has the property that it generates a maximum directly over discrete bodies as well as their edges. The width of a maximum, or ridge, is an indicator of depth of the contact, as long as the signal arising from a single contact can be resolved. This transformation is often useful at low magnetic latitudes because of the inherent problems with RTP, at such low latitudes (Blakeley and Simpson, 1986).

3.3.2. Euler Deconvolution

The objective of the Euler deconvolution process is to produce a map showing the locations and the corresponding depth estimations of geologic sources of magnetic or gravimetric anomalies in a two-dimensional grid (Reid, et al., 1990). Of many depth estimation techniques, the Euler deconvolution has become a popular choice because the method assumes no particular geological model. However, the conventional approach to solving Euler equation requires tentative values of the structural index (SI) preventing it from being fully automatic and assumes a constant background that can be easily violated if the singular points are close to each other (Dewangan, P., T. Ramprasad, M. V. Ramana, Desa, M., and Shailaja, B. 2007).

In general, the unknown regional field (B) can be approximated using Taylor series

(2)

$$B_{(x,y)} = B_0 + x\frac{\partial B}{\partial x} + y\frac{\partial B}{\partial y} + 0(2),$$

Where B0 is the constant background at the center of the specified window and O (2) represents higher-order terms in the Taylor series expansion. The anomalous field (T), can now be expressed as the deference between the observed (F) and regional (B) fields.

$$F = (x - x_0)\frac{\partial (F-B)}{\partial x} + (y - y_0)\frac{\partial (F-B)}{\partial y} + (z - z_{z0})\frac{\partial (F-B)}{\partial z} + n(F-B) = 0 \quad (3)$$

Euler equation becomes nonlinear and is solved linearly by assuming tentative values of the SI (Thompson, D. T, 1982; Reid, A. B et al., 1990). The Euler equation can also be solved linearly assuming constant background (Gerovska et al., 2005).

3.3.3. The Center for Exploration Targeting (CET) Porphyry Analysis Plug-In for Structures

The CET Porphyry Analysis Extension include (Holden E. J., et al., 2011):

i. The Circular Feature Transform plug-in;
ii. The Central Peak Detection plug-in;
iii. The Amplitude Contrast Transform plug-in; and
iv. The Boundary Tracing plug-in.

3.3.3.1. Circular Feature Transform

The circular feature transform (CFT) adapts an algorithm that calculates the radial symmetry transform(Loy and Zelinsky, 2003), which is designed to detect circular shaped features. The transform highlights the centers of elevated or depressed circular features by identifying where image gradients converge or diverge respectively. This plug-in permits the user to provide parameters specifying the radial size, circularity and completeness of features of interest.

3.3.3.2. Central Peak Detection

The Central Peak Detection plug-in locates the centers of circular features from a circular feature transform (CFT) output. This is achieved by suppressing non-maximum circularity responses within each neighborhood in the data while preserving the maximum value. Thresholding is then applied so that only significant feature centers are retained. The outputs are a database file and a polygon file. The database file specifies the circular feature centers, the radial symmetry strength, and the radius that resulted in the strongest response (in both cells and meters). The polygon file contains, for each feature location, the circle boundary that generated the strongest radial symmetry response. This enables visualization of the size of the detected circular features (Holden E. J., et al., 2011).

3.3.3.3. Amplitude Contrast Transform

The Amplitude Contrast Transform (ACT) plug-in measures the magnetic amplitude contrast of circular features at specific distances from their surroundings to highlight the feature boundaries. A circular feature in the magnetic contrast transform output will appear as a 'halo', which coincides with the circular rim of the feature (Holden E. J., et al., 2011).

3.3.3.4. Boundary Tracing.

The Boundary Tracing plug-in traces feature boundaries using an active contour algorithm (Williams and Shah, 1990). Active contours (snakes) are splines that are iteratively drawn to the feature boundaries using an energy minimizing technique. The spline energy is a function (over s control points of the spline) of two internal constraints that control the shape of the spline, namely the elasticity and curvature, and one image constraint that specifies feature boundaries that are being sought.

4 Results and Discussions

4.1. Interpretation of Structures Identified from Analytic Signal (AS) and Euler Deconvolution

The analytic signal map shown in (Fig. 4) was calculated for reduced to pole total magnetic intensity map (Fig. 3) to be used in detecting the edges of the source bodies in the study area. It is seen from the analytic signal map that the high magnetic intensity regions (magneta red color = 0.54 nT/km) and low magnetic intensity regions (various blue colors = 0.01 nT/km) can be easily distinguished compared to that seen in RTP map.

Analytic signal map shows that there might be strong anomalies due to intrusive bodies trending along NW direction. The major structural trends appear in the analytic signal map are NW (it can be easily noticed along whole study area) , WNW (clearly appears in the north western part of the study area), and NE (in the eastern and south western parts) directions.

The standard Euler deconvolution was applied to the reduced to pole total magnetic intensity map. For interpreting contacts, faults, dykes, structural index of 1 was found to give the best results (Fig.5). The results showed range of depths between 0.550 and 3.700km with trends of WNW, NW, NE, N and E directions.

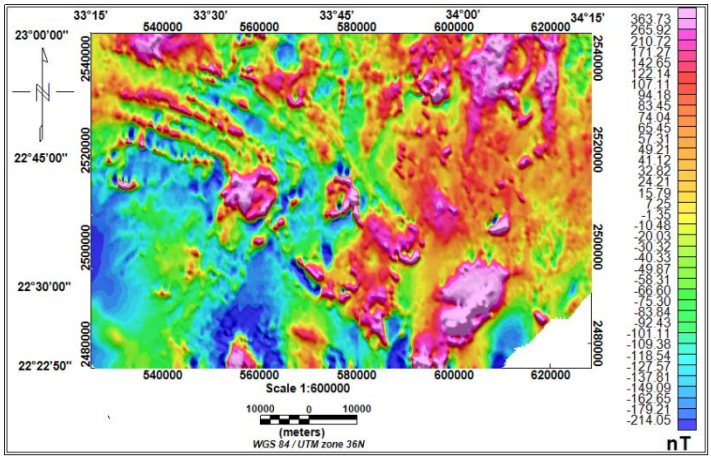

Figure (3): Reduced to Pole Total Magnetic Intensity Map.

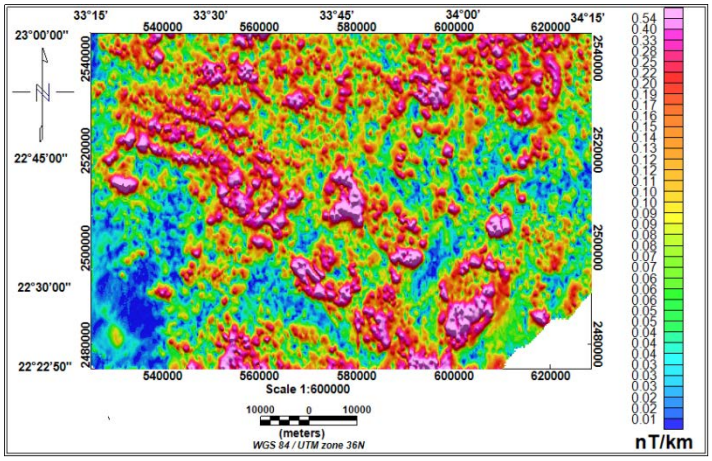

Figure (4): Analytic Signal Map.

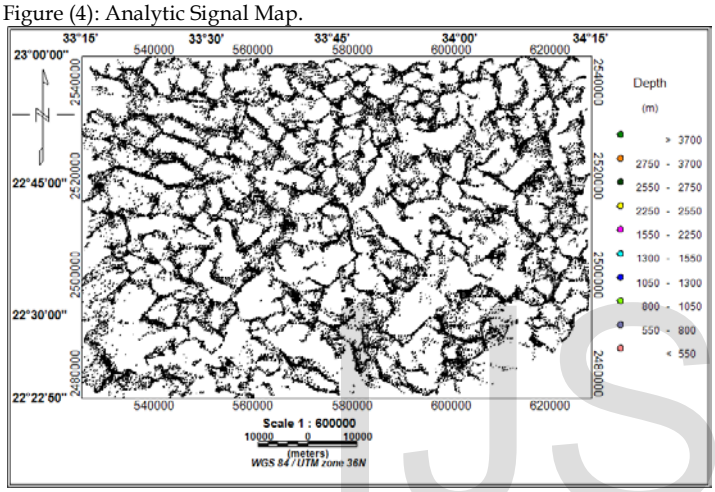

Figure (5): Euler Deconvolution With SI=1.

The clusters of Euler solutions in the range between 2750 m and 3700 m are observed along south and western part of the area while Euler solutions with depths more than 3700 m are mainly located over south western part of the study area suggesting deep structures in this part beneath the cretaceous sand stones. Other remaining Euler solution clusters between 550-2550 m are distributed over the entire area.

In general the resulting maps from applying standard Euler deconvolution method to the total magnetic intensity data show a very good clustering of symbols in linear and curved fashion indicating the nature of probable contacts between the rock units and expressing the different geometries of the causative bodies.

5.2. Application of CET Porphyry Analysis Plug-In and Results

Application of circular feature detection, central peak detection, amplitude contrast transform and boundary tracing produce the CET porphyry analysis map (Fig.6). The CET porphyry map allows comparison between the predicated and the known porphyry systems. The known systems are outlined in Black (*, ✱ , ×) and predicated in white triangles.

Wadi Allaqi area is known to contain numerous occurrences of porphyry-style mineralization. The predicated locations of CET porphyry systems closely match the location of the known deposits in the study area.

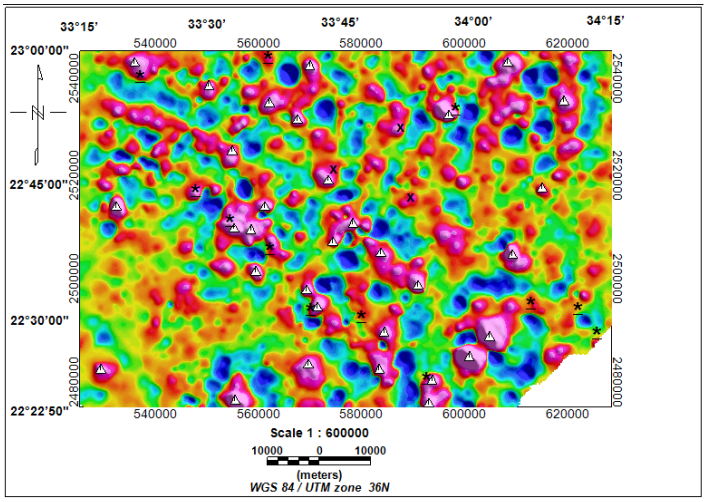

Figure (6): CET Porphyry Analysis Map.

From CET porphyry analysis map (Fig.6), we can notice that dike like structures that had been detected by the application of CET technique are structurally controlled along four main trend directions. These structural trends are NW-SE, WNW-ESE, NE-SW and N-S directions. Also, CET porphyry map shows a good correlation with the analytic signal map (Fig. 4) in the structural trends affecting Wadi Allaqi area and in the locations of porphyry intrusions.

5 Conclusion

From analytic signal map (Fig.6), Euler deconvolution map (Fig.7) and CET porphyry analysis map (Fig.8), the main structural trends observed within the study area are WNW-ESE, NW-SE, , NE-SW, N-S and E-W directions.

Using of Center for Exploration Targeting (CET) Plug-In Porphyry analysis to generate maps that highlights regions of porphyry-style mineralization from aeromagnetic data of the study area show there is a high correlation between the predicated locations of CET porphyry systems and the known deposits in the study area.

6 References

Abdelsalam, M.G., Stern, R.J., (1996): Sutures and shear zones in the Arabian–Nubian Sheild. Journal of African Earth Sciences 23, 289–310.

Blakely, R. J. and Simpson, R.W. (1986): Approximating edge of source bodies from magnetic or gravity anomalies. Geophysics, v. 51, pp. 1494 -1498.

Cella, F., Fedi, M., Florio, G., (2009): Toward a full multiscale approach to interpret potential fields. Geophysical Prospecting 57, 543-557.

Dewangan, P., T. Ramprasad, M. V. Ramana, Desa, M., and Shailaja, B., (2007): Automatic interpretation of magnetic data using Euler deconvolution with nonlinear background, Pure and Applied Geophysics, Vol.164; 2359-2372p.

El-Nisr, S.A., (1997): Late Precambrian volcanism at Wadi Allaqi, SE Desert, Egypt: evidence for continental arc/continetal margin environment. Journal of African Earth Sciences 24, 301–313.

Fedi, M., (2002): Multiscale derivative analysis: a new tool to enhance detection of gravity source boundaries at various scales. Geophysical Research Letters 29 (2). 1029 (16-1- 16-4).

Geologic map of Wadi Jabjabah Quadrangle, Egypt, (1996): Scale 1 : 250 000, EGSMA.

Gerovska, D., Stavrev, Y., and Arauzo-Bravo, M.J., (2005): Finite-difference Euler deconvolution algorithm applied to the interpretation of magnetic data from northern Bulgaria, Pure App. Geophys. 162, 591-608.

Gunn, P., (1997): Airborne Magnetic and Radiometric Survey. AGSO Journal of Australian Geology and Geophysics, 17,(2), 216p.

Gunn, P.J., Dentith, M.C., (1997): Magnetic responses associated with mineral deposits. AGSO Journal of Australian Geology and Geophysics 17, 145-158.

Holden,E.J., Fu, S.C., Kovesi,P., Dentith, M., Bourne, B., Hope, M., (2011): Automatic identification of responses from porphyry intrusive systems within magnetic data using image analysis. Journal of Applied Geophysics 74 (2011) 255–262.

Loy and Zelinsky (2003): “Fast Radial Symmetry for Detecting Points of Interest”, IEEE Transactions on Pattern Analysis and Machine Intelligence, Volume 25, Issue 8, pp. 959–973.

Macnae, J., (1995): Applications of geophysics for the detection and exploration of kimberlites and lampriotes. Journal of Geochemical Exploration 53, 213-243.

Mineral map of Egypt, Egypt, (1994): 1 : 2 000 000, EGSMA.

Nabighian, M. N., (1972): The analytic signal of two dimensional magnetic bodies with polygonal cross-section: its properties and use for automated anomaly interpretation. Geophysics, 37, 507-517.

Reeves, C.V., Reford, S.W., and Milligan, P.R., (1997): Airborne Geophysics: Old methods, new images in Gubbins, A.G.(ED). Proceedings of Exploration 97, Fourth Decennial International Conference on Mineral Exploration, pp. 13-30.

Reeves, C.V., (1998): Continental scale and global geophysical anomaly mapping: ITC Journal, 1998-2, p 91-98.

Reid, A.B., Allsop, J.M., Granser, H., Millet, A.J. & Somerton, I.W., (1990): Magnetic interpretations in three dimensions using Euler deconvolution Geophysics, 55, 80-91.

Roest, W. R., Verhoef, V., and Pilkington, M., (1992): "Magnetic interpretation using the 3-D analytic signal", Geophysics, v. 57, p. 116-125.

Stern, R.J., Kroner, A., Manton, W.I., Reischmann, T., Mansour, M., Hussein, I.M., (1989): Geochronology of Late Precambrian Hamisana shear zone, Red Sea Hills, Sudan and Egypt. Journal of the Geological Society of London 146, 1017–1030.

Stern, R.J., (1994): Arc assembly and continental collision in the Neoproterozoic East African Orogen: implications for consolidation of Gondwanaland. Annual Reviews of Earth and Planetary Sciences 22, 319–351.

Stern, R.J., Nielsen, K.C., Best, E., Sultan, M., Arvidson, R.E., Kroner, A., (1990): Orientations of Late Precambrian sutures in the Arabian–Nubian shield. Geology 18, 1103–1106.

Thompson, D. T. (1982), EULDPH: A new technique for making computer-assisted depth estimates from magnetic data, Geophys. 47, 31–37.

Williams and Shah (1990): “A Fast Algorithm for Active Contours”, Third International Conference on Computer Vision, pp. 592–595.

IJSER

IJSER